QCD Studies in the Breit Frame at HERA

D. Kant[a]

[a]Department of Physics,
Queen Mary & Westfield College,
Mile End Road, London E1 4NS

Fragmentation functions, invariant energy spectra and differential events shape spectra in Deep Inelastic Scattering are studied in the current region of the Breit frame. The data, taken by the H1 and ZEUS experiments at HERA, are compared with results from e^+e^- collisions and fragmentation universality is tested.

1. Introduction

The hadronic final state resulting from a partonic scattering process can be viewed to factorise into the partonic process itself followed by a subsequent hadronisation process. For large scales, the running coupling constant is small and hard scattering cross sections can be calculated reliably using perturbative QCD. However, the hadronisation process involves mass scales of the order of $\Lambda_{\rm QCD}$. At these scales, the running coupling constant is large and the perturbative picture breaks down. The fragmentation of partons into hadrons must therefore be described by means of a phenomenological model. Recent progress has been made in understanding this process within the framework of the Modified Leading Logarithmic Approximation (MLLA) complemented with the assumption of Local Parton Hadron Duality (LPHD).

Previous studies at HERA [1,2] have demonstrated that in ep interactions, particle production in the current hemisphere of the Breit frame is very similar to a single hemisphere of an e^+e^- collision when Q, the magnitude of the four momentum transfer, is taken to be equivalent to the centre of mass energy $\sqrt{s_{\rm ee}}$.

2. The Breit Frame

A particularly suitable frame of reference in which to study the recoiled quark with minimal contamination from target fragmentation effects is the Breit frame. Within the context of the Quark Parton Model, the purely space-like gauge boson γ/Z has longitudinal momentum $-Q$ and collides elastically with the incoming quark whose longitudinal momentum is $Q/2$. The struck quark is back-scattered into the current hemisphere with an equal but opposite momentum $-Q/2$, while the proton remnant fragments in the opposite hemisphere. Viewed in this reference frame, the four-momentum vector of the exchange boson defines a natural axis - the photon axis - in which to study particle spectra where the available energy for fragmentation in the current region is $Q/2$.

This situation can be compared with $e^+e^- \rightarrow q\overline{q}$ annihilation, where the available energy in one hemisphere, defined with respect to the thrust axis, has a mean value equal to $\sqrt{s_{\rm ee}}/2$.

3. Fragmentation Functions

One of the simplest distributions sensitive to gluon radiation is the single particle inclusive scaled momentum distribution, $D(x_p)$. Here, x_p is a measure of the fraction of momentum taken by the final state charged particles in the current hemisphere to the momentum of the initial parton $Q/2$ (QPM). The function characterises the complete process of final state parton shower development and non-perturbative hadronisation and is shown in Figure 1 for two different Q values. As the available energy for fragmentation increases, the phase space for gluon radiation increases and the likelihood of observing final state particles with a large share of the initial parton momenta gets smaller. Consequently, the function becomes softer, turning over as $x_p \to 0$, with increasing energy.

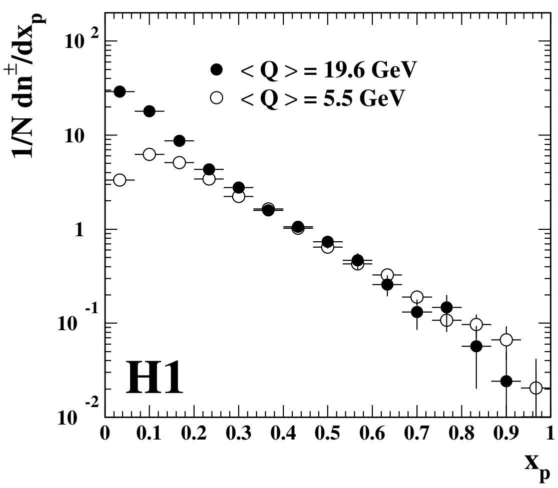

Figure 1. The scaled momentum distribution shown at two different values of momentum transfer.

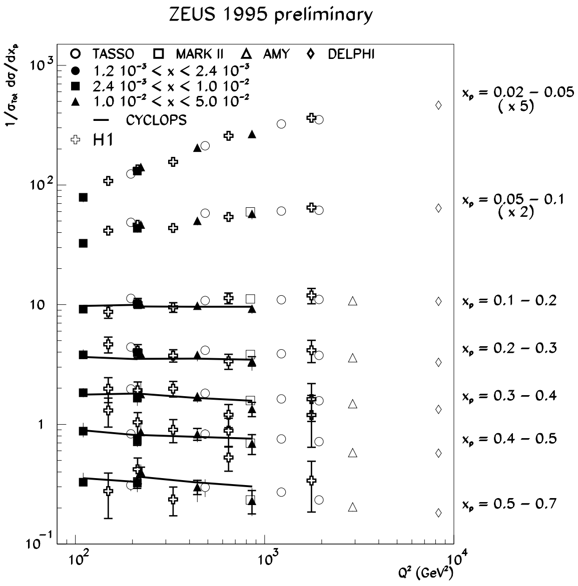

Figure 2. Scaling violation of the fragmentation function. The data points are from ZEUS and H1 which are compared with e^+e^- data and the predictions of CYCLOPS, a NLO calculation (solid line).

These violations may be studied in more detail [3,4] by examining the energy behaviour of the functions in intervals of x_p as shown in Figure 2. The data exhibit a rise with increasing Q^2 in the small x_p region which becomes flatter in the large x_p region. NLO calculations based on input fragmentation function distributions from fits to e^+e^- data [5] have recently become available [6] which provide a good description of the data ($x_p > 0.1$) at large values of Q^2. The observation of scaling violations in a single experiment should allow a measurement of the strong coupling constant at HERA. However, in order to get sufficient sensitivity to α_s, the data must extend into the larger Q^2 ($>> 10^3$ GeV^2) where NLO predictions are expected to be valid in the small x_p (< 0.1) region. Such a measurement would require increased statistics (≈ 250 pb^{-1}) [7] to yield a result comparable to the world average with a competitive error.

4. MLLA Predictions and the Humped backed Plateau

In order to examine the turn-over in the low x_p region more closely, the scaled momentum distributions are cast in terms of the variable $\xi = \ln(1/x_p)$. The expectation of the Modified Leading Logarithmic Approximation (MLLA) to perturbative QCD is that this distribution - in the neighbourhood of the peak - is an approximate Gaussian for the partons. This characteristic *hump-backed* plateau [8] is a direct consequence of gluon coherence which gives rise to a suppression of soft gluon radiation at wide angles in the particle cascade. In the absence of gluon coherence there is no suppression of soft particles and the spectra develop a shoulder in the low momentum (large ξ) region.

Assuming that the basic features of this distribution are preserved for the hadrons - Local Parton Hadron Duality (LPHD) - the growth of the peak and averaged charged multiplicity are expected to increase more slowly with energy than if the parton cascade is merely governed by longitudinal phase space. The fragmentation spectra cast in this variable are shown at two values of Q in Figure 3. The data shown are hump-backed and can be described by Gaussian fits.

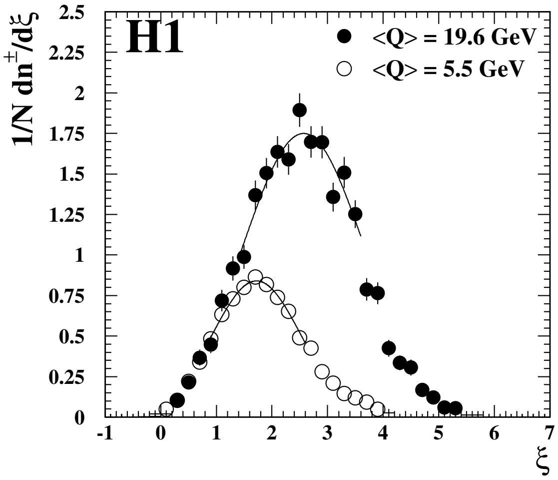

Figure 3. The scaled momentum distribution shown at two different values of energy. The solid lines are Gaussian fits to a limited region around the statistical means.

Assuming gluon coherence, the predicted behaviour of the peak and width with energy (Equations 1 and 2) is given in terms of a dimensionless variable $Y = \ln(Q/\Lambda_{\rm eff})$, where $\Lambda_{\rm eff}$ is an effective scale parameter.

$$\xi_{\rm peak} = 0.5Y + c_2\sqrt{Y} + d \qquad (1)$$

$$\xi_{\rm width} = \sqrt{Y^{3/2}/2c_1} \qquad (2)$$

The constants c_1 and c_2 are dependent on the number of flavours and colours in QCD and, d, is a slowly varying function with energy (assumed constant) containing all QCD diagrams beyond leading order. The energy evolution of the fragmentation function may then be summarised by the energy dependence of the peaks and widths presented in Figure 4. There is an excellent agreement between the ep and e^+e^- data [9–12]. The solid line is the result of a simultaneous fit to the H1 data only. Additionally the parameters of the fit ($\Lambda_{\rm eff} = 0.21 \pm 0.02$ GeV, $d = -0.43 \pm 0.06$) are in very good agreement with those determined in a similar analysis by the OPAL collaboration [10] ($\Lambda_{\rm eff} = 0.21 \pm 0.02$ GeV, $d = -0.32 \pm 0.06$).

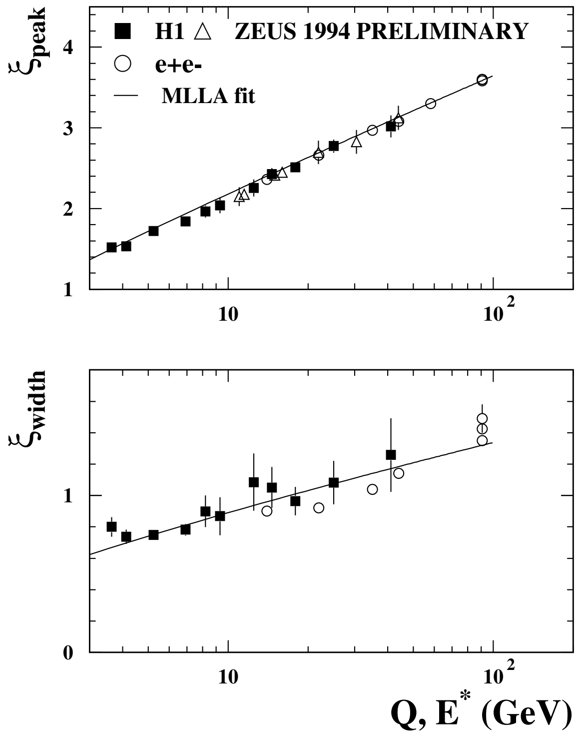

Figure 4. Energy evolution of the first and second moments of the fragmentation function shown for the H1 (closed squares), ZEUS (open triangles) and e^+e^- (open circles) data. The solid line is a simultaneous fit of the MLLA parameterisation to the H1 data only described in the text.

5. Charged Particle Multiplicities

The area under the fragmentation function is the averaged charged particle multiplicity and its behaviour with energy is shown in Figure 5. At high energies, there is a good agreement between the ep data and the data of e^+e^- (solid line). However, at lower energies where α_s is large, there is a significant shortfall.

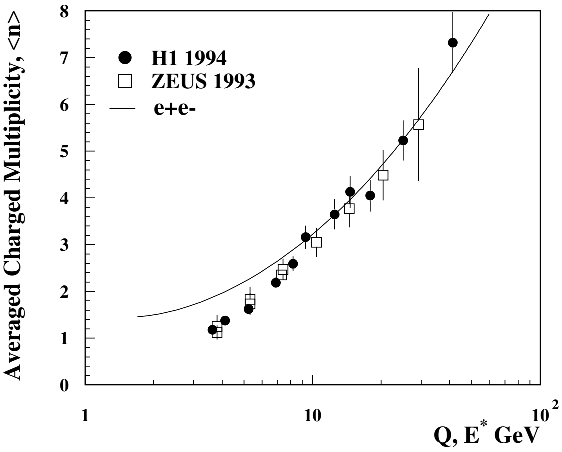

Figure 5. Average charged multiplicities for H1 (close circles) and ZEUS (open squares). The solid curve is a fit to many e^+e^- results as a function of the centre of mass energy, E^*

The full multiplicity distribution in the KNO [13] form is presented in Figure 6. In e^+e^- interactions at high energies ($\sqrt{s_{ee}} >$ 20 GeV) [14] the distribution shows approximate scaling. However, the upper plot shows that the distribution becomes narrower as Q^2 increases and hence a clear scaling violation is observed. The ep data at high momentum transfer are similar to e^+e^- data at high centre of mass energies. The lower figure shows that the low Q^2 data deviate significantly from e^+e^- data. Remarkably better agreement can be obtained if cuts are applied which reduce leading order QCD contributions, present in ep data but absent in e^+e^- interactions such as boson gluon fusion and initial state QCD compton. Details of these *flow selected* cuts can be found elsewhere [3]. A similar observation is made for the average charged particle multiplicity.

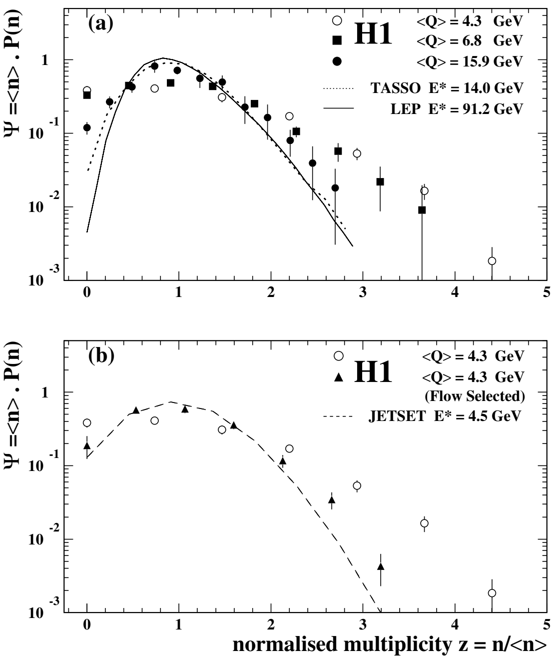

Figure 6. The KNO distribution for H1 data at different Q^2 compared with single hemisphere e^+e^- data (solid line) and Monte Carlo (JETSET [15] dashed).

6. Invariant Energy Spectra

Following recent developments [16] in perturbative QCD based on the MLLA, we examine for the first time in DIS the invariant energy spectra $(E/N)dn/d^3p$, shown in Figure 7 where dn/d^3p is the number of tracks in a given element of 3D momentum space and so represents a particle density. The expectation of the theory is that the production rate of soft particles should be approximately independent of the energy of the parent parton. Such scaling behaviour has also been demonstrated [17] in $\mathrm{e^+e^-}$ interactions over a wide range of centre of mass energies, in which the data move toward a common limit as the particle momenta become small.

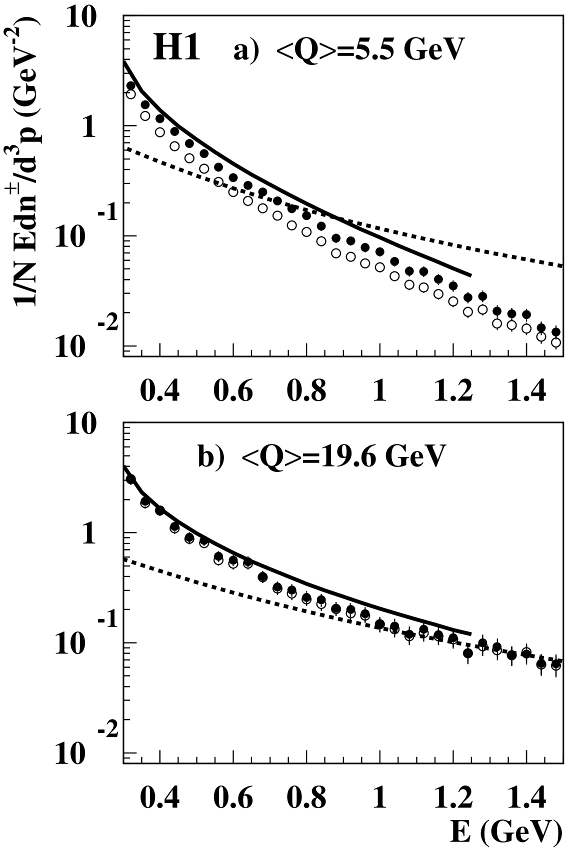

Figure 7. The invariant energy spectra for charged particles. The H1 data with (closed circles) and without (open circles) the flow selected cut are shown. The solid line is the prediction of MLLA + LPHD and the dashed line is the corresponding prediction for a non-running coupling constant, α_s.

The theoretical predictions solid/dashed curves are sensitive to the running of the strong coupling constant. Theoretical predictions that assume a fixed strong coupling (dashed line) within the particle cascade are not supported by this data.

7. Event Shape Distributions

Hadronic final states in deep inelastic scattering offer an ideal environment to study hadronisation phenomena and to measure the strong coupling constant over a wide range of momentum transfer Q in a single experiment. As in the case of e^+e^- interactions, event shape variables may be defined which characterise the hadronic final state. Such variables are infrared and collinear safe and have been calculated to $\mathcal{O}(\alpha_s^2)$ within perturbative QCD. In the analysis of [18], the thrust T_c and T_z, the jet broadening B_c and the jet mass ρ_c are examined. The definitions of these variables are given below, where the sums are over all hadron momenta p_h in the current region and, $\mathbf{n}_T$ and $\mathbf{n}$ are unit vectors along the direction of the thrust and photon axis respectively.

$$T_c = \max\frac{\Sigma_h|p_h.\mathbf{n}_T|}{\Sigma_h|p_h|} \tag{3}$$

$$T_z = \frac{\Sigma_h|p_h.\mathbf{n}|}{\Sigma_h|p_h|} \tag{4}$$

$$B_c = \frac{\Sigma_h|p_h\times\mathbf{n}|}{2\Sigma_h|p_h|} \tag{5}$$

$$\rho_c = \frac{M^2}{Q^2} = \frac{(\Sigma_h p_h)^2}{Q^2} \tag{6}$$

The normalised differential spectra for $1-T_c$ together with predictions from the LEPTO Monte Carlo are presented in Figure 8. As the available energy for fragmentation in the current region increases, the spectra become narrower and more peaked towards lower vales of $1-T_c$. A similar behaviour is seen for the other event shape variables which are not presented in this report. This observation can be explained in terms of the energy flow of the current system which becomes more collimated along the event shape axis as Q increases.

For each distribution, the energy dependence of the mean thrust $\langle 1-T_c\rangle$ are found to be in qualitative agreement with available e^+e^- data [19] at the scale $Q\equiv\sqrt{s_{\rm ee}}$, as shown in Figure 9.

Differences between the ep and e^+e^- data are most pronounced at low momentum transfer where the boson gluon fusion diagram is a large contribution to the neutral current ep cross section. These processes can give rise to events in which the current hemisphere is totally devoid of hadronic activity resulting in events in which there is no meaningful thrust. For BGF initiated process where there is hadronic activity, the energy flow is less collimated with respect to the photon axis. In these cases, the thrust axis can point in a direction such that the angle between the two axis is large. In extreme cases, the two axis can be perpendicular to one another. These complications do not arise in e^+e^- interactions where the thrust axis is calculated using all hadrons in the final state.

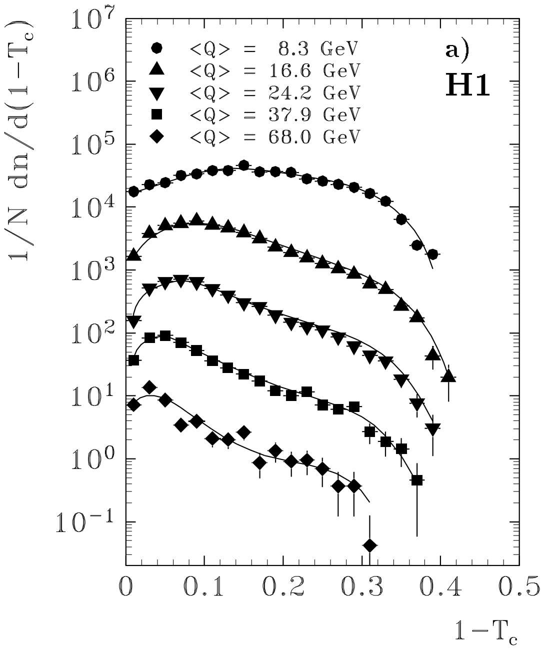

Figure 8. Differential event shape spectra for $1 - Tc$ as a function of Q. The data (full symbols) are compared with the LEPTO Monte Carlo (solid line). The spectra for $\langle Q \rangle = 8.3 - 68$ GeV are multiplied by factors of $10^n(n = 0, 4)$.

Within the theoretical framework, the energy

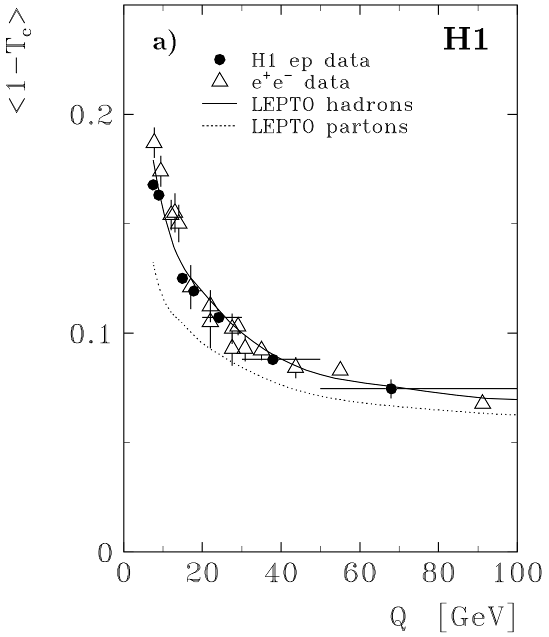

Figure 9. Mean of the differential thrust distribution, $\langle 1 - T_c \rangle$, as a function of Q compared with e^+e^- mean values at the centre of mass energy $\sqrt{s_{ee}}$.

dependence of the mean values can be attributed to both the logarithmic change in α_s with energy and power correction effects. The power corrections, which are expected to behave like $1/Q$, may be related to a universal soft gluon phenomena associated with the behaviour of the running coupling at small momentum scales [20]. Using the approach adopted in [21], the mean value of any infrared safe event shape variable $\langle F \rangle$ may be written as the sum of two contributions.

$$\langle F \rangle = \langle F \rangle^{\text{pert}} + \langle F \rangle^{\text{power}} \tag{7}$$

The perturbative term represents the second order QCD prediction in the $\overline{MS}$ scheme and can be performed with the MEPJET [22] and DISENT [23] Monte Carlo programs which treat ep scattering to $\mathcal{O}(\alpha_s^2)$ via single photon exchange. The power correction term contains a non-perturbative free parameter, $\overline{\alpha}_0$, which describes the effective behaviour of the strong coupling constant at small scales. Fits may then be performed to the data in order to determine both $\alpha_s(M_Z)$ and $\overline{\alpha}_0$. The results of the fits (solid line) are shown in Figure 10 and presented in Table 1 (statistical errors only). The dotted line is the prediction of the second order QCD calculation and shows that the power corrections are substantial at low values of Q. A discussion of the theoretical uncertainties in this analysis can be found elsewhere [18].

All event shape analyses give results consistent with each other for $\overline{\alpha}_0$ and $\alpha(M_Z)$. The remarkable similarity of $\overline{\alpha}_0$ between ep and e^+e^- experiments provides support for the concept of a universal power correction parameter discussed in [21].

8. Conclusions

Deep inelastic ep data analysed in the current region of the Breit frame have been presented. Charged particle distributions cast in the form of fragmentation functions show a clear scaling violation. The energy dependence of the moments of the functions have been compared with e^+e^- data using the MLLA formalism which provides a framework to compare fragmentation in different processes and energy ranges. The DIS data are consistent with a common limit in the invariant energy spectrum and theoretical prediction that assume a fixed strong coupling constant are not supported by the data. The results presented provide strong evidence in support of the universality of quark fragmentation. For the first time in deep inelastic ep scattering, the event shape variables thrust, jet broadening and jet mass have been studied. Using second order QCD calculations and a specific model to describe the influence of non-perturbative effects on hadronic final states, a QCD fit to the energy dependencies of the mean event shape variables has been performed in order to determine both α_s and $\overline{\alpha}_0$. The power corrections are found to behave as $1/Q$ and can be described by a common universal parameter $\overline{\alpha}_0$ whose values are consistent with those determined in e^+e^- experiments.

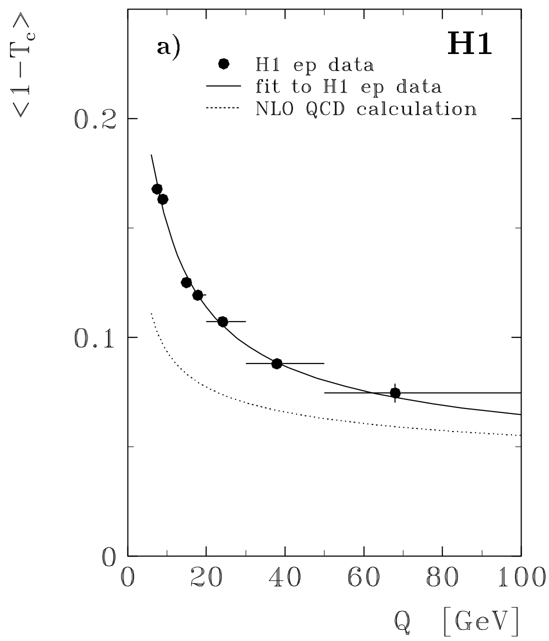

Figure 10. QCD fit (solid line) to the mean thrust $\langle 1 - T_c \rangle$. The dashed line is the second order QCD prediction provided by the DISENT Monte Carlo program.

REFERENCES

1. H1 Collaboration, S. Aid et al, Nucl. Phys. 445B (1995) 3.
2. ZEUS Collaboration, M. Derrick et al., Z. Phys. C67 (1995) 93.
3. H1 Collaboration, C. Adloff et al., Nucl. Phys. B 504 (1997) 3.
4. ZEUS Collaboration, DESY 97-183, Submitted to Physics Letters.
5. J. Binnewies et al., Z. Phys. C65 (1995) 471.
6. D. Graudenz, CERN-TH/96-52.
7. D. Graudenz, Prospects for a measurement of α_s via scaling violations of fragmentation functions in deeply inelastic scattering, Future Physics at HERA, Vol. 1, 533.
8. Yu.L. Dokshitzer, V.A. Khoze, A.H. Mueller and S.I. Troyan, "Basics of Perturbative

Table 1
Results on power correction parameters α_0 and the strong coupling constant $\alpha_s(M_Z)$ from fits to the energy dependence of the mean event shape variables that are listed in the first column. The errors presented are statistical only.

Observable	$\overline{\alpha}_0(\mu_I = 2\ \text{GeV})$	$\alpha_s(M_Z)$	χ^2/dof
H1 ep data			
$\langle 1 - T_c \rangle$	0.497 ± 0.005	0.123 ± 0.002	5.0/5
$\langle 1 - T_z \rangle /2$	0.507 ± 0.008	0.115 ± 0.002	8.5/5
$\langle B_c \rangle$	0.408 ± 0.006	0.119 ± 0.003	5.3/5
$\langle \rho_c \rangle$	0.519 ± 0.009	0.130 ± 0.003	3.1/5
e^+e^- data			
$\langle 1 - T_{ee} \rangle$	0.519 ± 0.009	0.123 ± 0.001	10.9/14
$\langle M_H^2/s \rangle$	0.431 ± 0.020	0.115 ± 0.002	7.8/14

QCD" Editions Frontiérs (1991); L.V. Gribov, Yu.L. Dokshitzer, V.A. Khoze and S.I. Troyan, Phys. Lett. 202B (1988) 276; Ya.I. Azimov,Yu.L. Dokshitzer, V.A. Khoze, and S.I. Troyan, Z. Phys. C31 (1986) 213, Z. Phys. C27 (1985) 65.

9. TASSO Collaboration, W. Braunschweig et al., Z. Phys. C47 (1990) 187.
10. OPAL Collaboration, M.Z. Akrawy et al., Phys. Lett. B247 (1990) 617.
11. L3 Collaboration, B. Adeva et al., P. Lett. B259 (1991) 199.
12. TOPAZ Collaboration, R. Itoh et al., Phys. Lett. B345 (1995) 335.
13. Z. Koba, H.B. Nielsen and P. Olesen, Nucl. Phys. 40B (1972) 317.
14. TASSO Collaboration, W. Braunschweig et al., Z. Phys. C45 (1989) 193; DELPHI Collaboration, P. Abreu et al., Z. Phys. C56 (1992) 63.
15. T. Sjöstrand, Comp. Phys. Comm 82 (1994) 74; T. Sjöstrand, CERN-TH 7112/93 (revised August 1995).
16. V.A. Khoze and W. Ochs, Int. Journ. Mod. Phys. A12, (1997) 2949-3119.
17. V.A. Khoze, S. Lupia and W. Ochs, Phys. Lett. B 394 (1997) 179-187.
18. H1 Collaboration, Phys. Lett. B406 (1997) 256-270.
19. PLUTO Collaboration, Ch. Berger et al., Z. Phys C 12 (1982) 297; Mark II Collaboration, A. Peterson et al., Phys. Rev D 37 (1988) 11 and Z. Phys. C 47 (1990) 187; AMY Collaboration, Y.K. Li et al., Phys. Rev D 41 (1990) 2675; DELPH Collaboration, P. Abreu et al., Z. Phys. C 73 (1997) 229.
20. Yu.L. Dokshitzer and B.R. Webber at this conference.
21. B.R. Webber, Proceedings Workshop on DIS and QCD, Paris (1995), editors J.F Laporte and Y. Sirois, 115; M. Dasgupta and B.R Webber, Cavendish-HEP-96/5 and hep-ph/9704297.
22. E. Mirkes and D. Zeppenfeld, Phys. Lett. B 380 (1996) 205 and hep-ph/9511448.
23. S. Catani and M. Seymour, Nucl. Phys. B 485 (1997) 291 and hep-ph/9605323.